Production of thin-layer silicon alloys and their application in solar-hydrogen energy☆

Bakhtiyar A. Najafov [a], Shukur N. Nasirov [b,*], Shamsi N. Nasirov [c], Nijat M. Verdiyev [d]

[a] Institute of Radiation Problems of the Ministry of Science and Education, Az 1143, Azerbaijan, Baku, B. Vahabzade st., 9
[b] Azerbaijan State Oil and Industry University, Az 1010, Azerbaijan, Baku, Azadlig Ave., 16/21
[c] Baku Engineering University, Az 0102, Azerbaijan, Khirdalan, st. Hasan Aliyev, 120
[d] Azerbaijan State Oil and İndustry University, Az 1010, Azerbaijan, Baku, Azadlig Ave., 16/21

ABSTRACT

Exactly 50 years have passed since the beginning of the active phase of hydrogen energy (since 1974). The start of hydrogen energy in the 20th century was given by the efforts of the Patriarch of hydrogen energy, Professor T. N. Veziroglu. In the early works of Professor T.N. Veziroglu, the direction of solar-hydrogen energy already appears as the cleanest energy for improving the quality of life on the planet.

The development of solar energy is carried out fantastically quickly. In 2023, 428 GW of solar energy were added, which is 76% more than the same period last year, as a result of which the total installed solar capacity worldwide reached 1.6 TW.

An important direction of the solar-hydrogen system is the work to increase the efficiency of solar photovoltaic panels.

In this work, various parameters of films of amorphous and nanocrystalline silicon-carbon alloy (a-nc-$Si_{1-x}C_x$:H ($x = 0–1$)) doped with phosphorus (PH_3) and boron (B_2H_6) are investigated. The properties of these films obtained on various substrates of quartz, glass and silicon with a coating of Fe, Al, Pd, Ni, Ti, Ag, are studied. The morphology of the obtained nanotubes is studied using transmission electron microscopy (TEM). The structural properties of the films are also studied using infrared spectroscopy and X-ray diffraction. Cascade solar cells with an area of $S = 1.0$ cm^2 and an efficiency of 14.09% are created.

Solar photocells made of amorphous and nanocrystalline silicon-carbon alloy currently have the highest warranty resource - up to 35 years. This allows for long-term investments in the use of land that has a low cost with high benefit. At the same time, a good basis is created for the intensive development of solar-hydrogen energy.

1. Introduction

Exactly 50 years have passed since the beginning of the active phase of hydrogen energy (since 1974). The start of hydrogen energy in the 20th century was given by the efforts of the Patriarch of hydrogen energy, Professor T.N. Veziroglu [1–7]. In the early works of Professor T.N. Veziroglu, the direction of solar-hydrogen energy already appears as the cleanest energy for improving the quality of life on the planet [8–14]. The development of solar energy is carried out fantastically quickly. In 2023, 428 GW of solar energy were added, which is 76% more than the same period last year, as a result of which the total installed solar

capacity worldwide reached 1.6 TW. There are currently several hundred solar-hydrogen stations in the world. For example, Australia, which leads in the number of such stations, has 96 facilities. In general, the number of green hydrogen production projects (Fig. 1) continues to grow around the world.

Hydrogen-backed photovoltaic power generation systems (HBPPS) are a promising area in the field of renewable energy [15–17]. They combine photovoltaic panels for generating electricity and hydrogen batteries for storing it. Such systems are used to ensure a stable power supply in conditions of variable solar activity. They are used in residential buildings, commercial buildings, and industrial facilities where a

Fig. 1. Solar-Hydrogen Energy. (provided to the authors on 15.11.2024 for printing in IJHE from the archive of Fermaltech Montenegro Limited, made by A.L. Gusev using Designer. On the DALL E 3 platform.)

reliable and environmentally friendly power supply is required. Hydrogen-backed photovoltaic HBPPS are actively developing in countries with high levels of solar insolation and a desire to decarbonize the energy sector. Among the leaders are Germany, Japan, the USA, China, and Australia. Exact data on the number and capacity of such systems vary depending on the region and specific projects. In general, the capacity of hydrogen-backed photovoltaic systems can reach several megawatts, which makes it possible to provide energy to large facilities and even small towns. The volumes of hydrogen produced by photovoltaics depend on the capacity of the installations and operating conditions.

Hydrogen energy is currently in the active development stage, and the volumes of hydrogen production from renewable sources are gradually increasing [18–20].

Solar-hydrogen energy has a number of significant advantages that make it attractive for use in the future:

1. Environmental friendliness: The production and use of hydrogen does not emit carbon dioxide and other harmful emissions, which helps reduce air pollution and combat global warming.
2. Renewability: Solar energy is an inexhaustible source, making it a sustainable and reliable option for long-term energy supply.
3. Energy efficiency: Hydrogen has a high energy capacity per unit mass, which allows for efficient storage and transportation of energy.
4. Reduced dependence on fossil fuels: The use of hydrogen can significantly reduce dependence on oil and coal, which contributes to energy security and stability.
5. Storage and transportation: Hydrogen can be stored in large quantities and transported over long distances, making it convenient for use in various regions and conditions [21–25].
6. Integration with other renewable energy sources: Solar hydrogen systems can be integrated with other renewable sources such as wind energy, increasing their overall efficiency and reliability [26].

Modern solar photovoltaic systems have efficiencies in the range of 15%–30% in mass production. This figure depends on the type of materials and technologies used:

a) Amorphous silicon (A-Si): efficiency of 14–16%.
b) Polycrystalline silicon (Poli-Si): efficiency of 19–21%.
c) Monocrystalline silicon (Mono-Si): efficiency up to 24%.
d) Cadmium telluride (Cd–Te): efficiency slightly lower than polycrystalline, but with more stable performance.
e) Rare earth copper indium gallium sulfide (CIGS): efficiency up to 40% in laboratory conditions.

The efficiency of hydrogen production in solar hydrogen stations varies, but on average is around 20%. This means that 20% of solar energy is converted into hydrogen. Hydrogen fuel cells, used to convert hydrogen back into electricity, can achieve efficiency up to 60%.

Warranty periods for photovoltaic panels depend on their type and manufacturer:

1) Monocrystalline panels: warranty from 25 to 30 years. They can retain up to 80% of their original capacity after 25 years of operation.
2) Polycrystalline panels: warranty from 20 to 25 years. They can also retain up to 80% of their capacity after 20–25 years.
3) Thin-film panels: warranty from 10 to 20 years, depending on the technology and manufacturer.

Evaluating the role of famous scientists in the development of solar-hydrogen energy technologies today, it is important to emphasize the significant contribution to the development of solar-hydrogen energy of 12 scientists:

1. Edmond Becquerel: discovered the photovoltaic effect in 1839, which became the basis for the development of solar technology. Edmond Becquerel, a French physicist, discovered the photovoltaic effect in 1839 when he was just 19 years old. He observed that certain materials could produce a small electric current when exposed to light. This discovery laid the groundwork for the development of solar technology. Becquerel's experiment involved immersing two electrodes in a conductive solution and exposing them to light, which generated a voltage. Although the efficiency of his early experiments was very low, his work was crucial in understanding how light can be converted into electrical energy.

This foundational discovery eventually led to the development of modern photovoltaic cells, which are now widely used to harness solar energy for various applications.

2. William Grylls Adams and Richard Evans Day: Observed the photovoltaic effect in selenium in 1876. In 1876, William Grylls Adams and his student Richard Evans Day made a significant discovery by observing the photovoltaic effect in selenium. They found that selenium produced electricity when exposed to light, demonstrating that a solid material could convert light into electrical energy without the need for heat or moving parts [27]. This discovery was crucial in the development of modern solar cells and laid the groundwork for future advancements in photovoltaic technology.
3. Charles Fritts: created the first working photovoltaic cell using selenium in 1883. Charles Fritts is credited with creating the first working photovoltaic cell in 1883. He achieved this by coating selenium, a semiconductor, with a thin layer of gold. This early solar cell had an energy conversion efficiency of about 1% [28]. Despite its low efficiency, Fritts' invention was a significant milestone in the development of solar technology, marking the birth of photovoltaics—the conversion of light into electricity.
4. Albert Einstein was awarded the Nobel Prize in Physics in 1921 for his discovery of the photoelectric effect [29].

This groundbreaking work demonstrated that light could be understood as consisting of particles, or "quanta," which we now call photons (Fig. 2). Einstein's theory explained how light of a certain frequency can
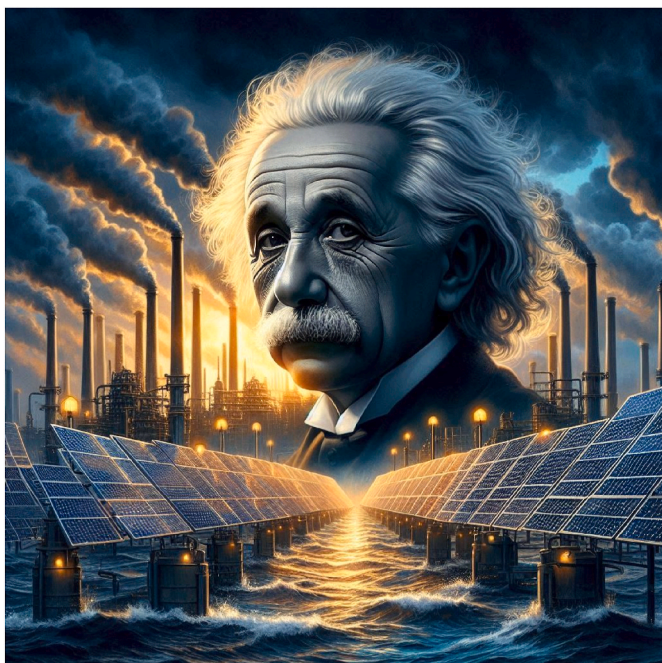
Fig. 2. The Impact of Albert Einstein's Work on the Development of Solar-Hydrogen Energy. (provided to the authors on 15.11.2024 for printing in IJHE from the archive of Fermaltech Montenegro Limited, made by A.L. Gusev using Designer. On the DALL E 3 platform.)

Fig. 3. Solar Hydrogen Plant. (provided to the authors on 15.11.2024 for printing in IJHE from the archive of Fermaltech Montenegro Limited, made by A.L. Gusev using Designer. On the DALL E 3 platform.)

eject electrons from a material, a phenomenon that classical wave theory couldn't account for [30] (see Fig. 3).

This discovery was pivotal in the development of quantum mechanics and has had a lasting impact on the field of physics, including the development of photovoltaic technology used in solar cells today [31].

5. Daryl Chapin, Calvin Fuller, and Gerald Pearson: Developed the first silicon photovoltaic cell at Bell Labs in 1954. Daryl Chapin, Calvin Fuller, and Gerald Pearson were instrumental in developing the first practical silicon photovoltaic cell at Bell Laboratories in 1954. This groundbreaking invention marked a significant milestone in the field of solar energy. The cell had an initial efficiency of about 6%, which was a remarkable achievement at the time [32].

Their work laid the foundation for modern solar technology, leading to the development of photovoltaic solar panels that are widely used today. This innovation has had a profound impact on renewable energy, helping to reduce reliance on fossil fuels and combat global warming [33].

6. Turhan Nejat Veziroglu - development of the foundations of solar-hydrogen energy for the Hydrogen Civilization (1974–2024). Turhan Nejat Veziroğlu was a pioneering figure in the field of hydrogen energy, often referred to as the "father of the hydrogen economy" [34–36].

His work laid the foundation for the integration of solar energy and hydrogen systems, which he believed could lead to a sustainable and clean energy future [34].

In 1974, Veziroğlu organized one of the first conferences on hydrogen energy, which marked the beginning of his extensive efforts to promote hydrogen as a key energy carrier [35]. He established the Clean Energy Research Institute at the University of Miami and was instrumental in founding the International Association for Hydrogen Energy [36]. His vision of a "Hydrogen Civilization" emphasized the use of hydrogen produced from renewable sources like solar energy to replace fossil fuels [37].

Veziroğlu's contributions have had a lasting impact on the development of hydrogen technologies and their integration with solar systems, paving the way for advancements in sustainable energy solutions [38–41].

7. Martin Green: known for his research into high-efficiency silicon solar cells. Martin Green is a renowned figure in the field of photovoltaics, particularly known for his pioneering work on high-efficiency silicon solar cells. He has made significant contributions to improving the energy conversion efficiency of silicon solar cells, achieving over a 50% relative improvement from 1983 to 2008 [42].

One of his most notable inventions is the Passivated Emitter and Rear Cell (PERC), which has become a dominant technology in the solar industry due to its high efficiency and cost-effectiveness [43].

His team at the University of New South Wales (UNSW) has held the world record for silicon cell efficiency multiple times, with efficiencies reaching up to 22.8% [44].

Green's work has had a profound impact on the commercial solar cell market, making solar energy more accessible and affordable worldwide.

8. Masatoshi Nakanishi: worked on the development of hydrogen fuel cells and their integration with solar systems. Masatoshi Nakanishi has made significant contributions to the development of hydrogen fuel cells and their integration with solar energy systems. His work focuses on creating efficient and sustainable energy solutions by combining solar photovoltaic (PV) technology with hydrogen fuel cells. This hybrid approach aims to harness solar energy to produce hydrogen, which can then be used in fuel cells to generate electricity [45].

One notable project involves the techno-economic analysis of hybrid solar PV/hydrogen/fuel cell systems for green mobile communication [45]. This research explores the feasibility of using these hybrid systems to power cellular base stations, reducing environmental impact and

reliance on fossil fuels.

Nakanishi's efforts are part of a broader movement towards sustainable energy solutions, leveraging the strengths of both solar and hydrogen technologies to create more reliable and eco-friendly power sources.

9. Alexander L. Gusev has made significant contributions to the field of hydrogen energy and alternative energy systems. He is known for developing the Concept of Alternative Energy and Ecology (CAEE) from 2000 to 2024. This concept focuses on integrating various renewable energy sources and improving the efficiency and safety of hydrogen systems [46].

Gusev's work includes advancements in the reception, storage, delivery, and transportation of hydrogen. He has also contributed to enhancing the safety and reliability of hydrogen systems, which are crucial for their widespread adoption [47,48]. His research has been published in numerous scientific journals, and he has been involved in various international collaborations to promote sustainable energy solutions [48].

10. John Bockris: one of the pioneers in the field of electrochemistry and hydrogen energy. John O'Mara Bockris was indeed a pioneering figure in electrochemistry and hydrogen energy. Born in 1923, he made significant contributions to the field throughout his career. Bockris is well-known for coining the term "hydrogen economy" in the 1970s, which describes a system where hydrogen is used to transport and store energy from renewable sources [49].

He published around 700 papers and numerous books, covering topics such as bioelectrochemistry, photoelectrochemistry, and pulse electrolysis [50]. Bockris also explored controversial areas like cold fusion and transmutation later in his career [51].

His work laid the foundation for many modern advancements in electrochemistry and sustainable energy solutions.

11. Sergey A.Khudjakov: contribution to the theory and practice of on-board solar-hydrogen systems using hydrogen fuel cells. Sergey A. Khudjakov has made notable contributions to the development of on-board solar-hydrogen systems, particularly focusing on the integration of hydrogen fuel cells. His work encompasses various aspects of hydrogen technology, including the reception, storage, delivery, and transportation of hydrogen to consumers [52].

Khudjakov's research has been instrumental in enhancing the safety and reliability of hydrogen systems, which are critical for their practical application in transportation and other sectors. His efforts have helped advance the technology needed to efficiently store and use hydrogen in fuel cells, making it a viable option for sustainable energy solutions [52].

12. Klaus Schaefer: made a significant contribution to the development of hydrogen production technologies using solar energy. Klaus Schaefer has indeed made significant contributions to the development of hydrogen production technologies, particularly focusing on the use of solar energy. As the Chief Technology Officer of Covestro, he has been involved in various initiatives aimed at integrating renewable energy sources with hydrogen production [53]. His work emphasizes the importance of sustainable and efficient methods for generating hydrogen, which is crucial for the transition to a clean energy economy [53].

These scientists played a key role in the development of technologies used in solar-hydrogen energy today.

An important direction of the solar-hydrogen system is the work to increase the efficiency of solar photovoltaic panels.

The study of amorphous and nanocrystalline silicon-carbon a-нк-Si$_{1-x}$C$_x$:H $(x = 0-1)$, obtained by various methods and under various conditions, is of great interest in the field of nanoelectronics. In these films, the process of appearance of nano-sized effects is of great interest, which include: clusters, nanowires, nanotubes, nanoparticles, fullerenes, endofullerenes, quantum dots, quantum wells, graphenes, etc. The introduction of hydrogen plays a huge role in obtaining the film and is of particular interest.

To obtain such films, various types of substrates are selected, such as: quartz, glass, crystalline and monocrystalline silicon, etc.

There are a number of works devoted to obtaining a-nc-Si$_{1-x}$C$_x$:H, ($x = 0 \div 1$) and creating photoelectric converters based on them [54–68, 77,78]. Films obtained by magnetron sputtering, rapid thermal treatment, laser annealing and ion implantation are shown in Refs. [54–58]. In work [59] it was shown that in nanocrystalline SiC films with a thickness of 0.5–1 μm, obtained in 80% H$_2$ + 20% Ar plasma on a quartz substrate, with an increase in the substrate temperature from 200 to 600 0C, an increase in the density of SiC nanocrystals is observed, the average size of which was ~12 ÷ 24 nm. It was found that in films obtained from a gas mixture of SiH$_4$+H$_2$+PH$_3$ or SiH$_4$+H$_2$+B$_2$H$_6$ on a quartz or silicon substrate, with an increase in the concentration of PH$_3$, the average grain size (d) and the proportion of crystalline grains in volume (V$_C$) decrease. When doped with boron, with an increase in the concentration of B$_2$H$_6$, the value of d does not change, but V$_C$ increases [59]. The studies have shown that (H$_3$)$_3$SiCl can be used as a source of components for the synthesis of SiC [60]. However, films synthesized from its vapors are characterized by an excess of carbon. Depending on the synthesis temperature, localized carbon can be presented in both an amorphous and a nanocrystalline state. An increase in the synthesis temperature leads to a general increase in the degree of crystallinity of SiC films, the minimum temperature is T = 870^{0}C [60].

Electrical properties and current-induced structural changes of carbon nanotubes containing Cu nanorods were studied using transmission electron microscopy. The diameter and length of the nanotube with the rod are 18 and 256 nm, respectively, and the thickness of the graphite layer is ~1 nm. When a bias of 1.4 V is applied, the current in the tube increases to 10 μA (current density $4,0 \cdot 10^6$ A/cm^2) and simultaneously the nanorod begins to move towards the end of the tube. The specific resistance of the nanotube and nanorod is $3,0 \cdot 10^{-5}$ and $11,2 \cdot 10^{-4}$ Ohm m, respectively [61].

Hydrogenated nanocrystalline p-type silicon (nc-Si:H) with high conductivity was obtained by the method of RF-plasma-stimulated CGVO at medium power, high pressure and low substrate temperature. When studying the optoelectronic and structural properties of the obtained material, it was found that the films consist of nanocrystallites embedded in an amorphous SiHx matrix. Solar cells of the n-i-p type obtained on the basis of the films have an open-circuit voltage of 0.9 V, a fill factor of 0.7 and an efficiency of 9.0% [62]. At present, the efficiency of solar cells obtained on the basis of nanocrystalline films reaches 14%. The paper [63] studies the use of single-wall carbon nanotubes (CN) in photosensitive devices in combination with Si. Heterojunction solar cells based on the CN/Si structure have an efficiency of about 14% due to the use of CN photoactivity. Sensitive elements of gas nanosensors are also manufactured based on carbon nanotubes [64]. Experiments show that by changing the process parameters and conditions, amorphous films can be deposited on various structural phases. In addition, depending on the deposition conditions, both the film structures themselves and their optoelectronic properties strongly depend on the deposition rate, substrate temperature, substrate type, and geometry of the metal coatings.

The paper considers some parameters of thin films of amorphous and nanocrystalline silicon – carbon a-nc-Si$_{1-x}$C$_x$:H, ($x = 0 \div 1$). The mechanism of doping of this film with phosphorus (PH$_3$) and boron (B$_2$H$_6$) is also considered. The method of transmission electron microscopy (TEM) was used to study the morphology of the obtained nanotubes, the length of which, depending on the deposition conditions, is 1 ÷ 4 μm. The

structural properties of the films were analyzed by IR spectroscopy and X-ray diffraction (XRD). It was noted that, depending on the conditions of film production, such a change in parameters occurs, which is characteristic of nanocrystalline thin films.

NOMENCLATURE

Nomenclature	
Abbreviation table	
Letters of the Latin alphabet	
t	Temperature
d	film thickness
Cu	Nano rod
$n\text{-}i\text{-}p$	Solar cells $n\text{-}i\text{-}p$
XRD	X-ray diffraction
n	Refractive index
IR	Infrared
W_{rf}	Gas decomposition frequency
T_a	Hydrogen evolution temperature
J_p	x-ray scattering
$Torr$	Torricelli, gas pressure
E_a	Activation energy of electrical conductivity in the layer
$E_{g\ opt}$	Optical absorption limit
$h\nu$	The frequency of incident light
c	Speed of light
CN	Carbon nanotubes
$Å$	Deposition rate
$PH3$	Doped phosphorus
$Si\text{-}H2$	Dihydride complexes
R	Radius of the sphere of volume in which the dipole is located
N_S	Spin density number
T	Transmission of light of a specified wavelength
m	Reduced mass of a dipole
$e*$	Effective charge
eV	electron volt
$°C$	degree celsius
Letters of the Greek alphabet	
μm	Wavelength of light
μA	Unit of electric current
θ	Incident beam of angle
δ	Average crystallite size
Δ	Half-width of x-rays
γ	Frequency
ΔE	Activation energy
ω	Oscillation frequency
$(\alpha h\nu)^{1/2}$	Dependence that determines the optical absorption limit
$const = 4\pi/nc$	Fixed number
$\mathbf{V_\infty}$	Circuit voltage
$\boldsymbol{\alpha}$	Optical absorption coefficient
ξ	Fill factor
ν	Sedimentation rate
$\Delta\omega$	Absorption band shift
ε	Dielectric constant
λ	Wavelength
Superscripts and subscripts	
E_0	Bandgap width
V_C	Proportion of crystalline grains of volume
n_{sub}	Index of refraction of the substrate
n_{film}	Refractive index of the sheet
T_s	Substrate temperature
J_W	Integral absorption of the rocking mode for films
J_{sc}	Short-circuit current density
Abbreviations	
TEM	Transmission electron microscopy
$SWCNT$	Single wall carbon nanotubes
$DSCN$	Double-stage carbon nanotubes
$MWCNT$	Metallic multi-wall carbon nanotubes
RF	Radio frecansu-plasma-stimulated
ITO	Indium-tin oxides
CE	Collection efficiency
EPR	Electron paramagnetic resonance
HF	High frequency
$MASD$	Oscillator strengths by the silane decomposition method at direct current
FAS	Photoacoustic spectroscopy

(continued on next column)

(continued)

Nomenclature	
Abbreviation table	
$PCVDM$	Plasma chemical vapor deposition method
Chemical symbols	
$a\text{-}нк\text{-}Si_{1\text{-}x}C_x{:}H,\ (x = 0 \div 1)$	Gas mixture
$a\text{-}nc\text{-}Si1\text{-}xCx{:}H\ (x = 0\text{--}1)$	Gas mixture
Fe	Iron sole
Al	Aluminum contact
Pd	Palladium contact
Pt	Platinum contact
Ni	Nickel contact
Ti	Titanium contact
$B2H6$	Alloyed boron
SiC	
H_2	Hydrogen
Ar	Argon
$SiH_4+H_2+PH_3$	Silicon + hydrogen + phosphorus
$SiH_4+H_2+B_2H_6$	Silicon + hydrogen + boron
PH_3	Phosphorus
$\alpha\text{-}Si{:}H$	Amorf-silicon-hydride
$Si\text{-}H$	Silicon-hydride
Si	Silicon
Ge	Germanium
N_H	Number of hydrogen atoms
C	Carbon
$(H_3)_3SiCl$	Gas mixture- silicon chloride hydrogen
Ag	Silver
CH_4	Methane
Physical and chemical dimensions	
sm^3/min	cubic centimeter minute
sm^2	Square centimeter
Nm	nanometer
$Ohm\ m$	ohm per meter- it is a unit of resistance
V	volt
Wt	watt
Wt/sm^2	watt per square centimeter
W	Power
Other designations	
$etc.$	Abbreviation of the Latin phrase et cetĕra, meaning "and others", "and the like", "and so on"
$\%$	Percent
$IKS\text{-}21\ (İR\text{-}21)$	Spectrometer
$atm.$	atmosphere

2. Comparative analysis of analogues and prototypes

1. Study of the influence of deposition conditions. In the dissertation of Dmitry Mikhailovich Mitin, the influence of deposition conditions, such as working gas pressure, on the structure and properties of thin films of amorphous silicon is studied [65].
2. Formation of titanium dioxide films: the work of D.E. Shashin and D. S. Vladimirov considers the method of reactive magnetron sputtering for obtaining titanium dioxide films, which can also be applied to silicon-carbon films [66].
3. International Journal of Applied and Fundamental Research: this journal publishes studies devoted to various parameters of films of amorphous and nanocrystalline silicon-carbon alloy doped with phosphorus and boron [67].
4. These works help to better understand the processes and parameters that affect the properties of the resulting films, which is important for their further application in various fields.

3. Statement of the scientific problem

A number of analyzed works by various researchers show the prospects of solar cells based on thin-layer silicon alloys. The purpose of this work was to conduct experiments to obtain films of amorphous and nanocrystalline silicon carbon deposited by reactive magnetron

sputtering. The experimental plan included changing the process parameters: substrate temperature, film deposition rate, RF discharge power in order to determine the effect on the physical properties of amorphous and nanocrystalline silicon carbon.

The aim of the work was also to conduct studies that would confirm the possibility of using a-Si1-xCx:H and nc-Si films as materials for creating cascade solar cells and the possibility of using them in micro- and nanoelectronics.

4. Solar-hydrogen plants and their development prospects

Solar-hydrogen plants hold significant promise for the future of renewable energy. Here are some key development prospects:

1. Technological Advancements
   - Efficiency Improvements: Advances in photovoltaic (PV) technology and electrolyzers are increasing the efficiency of solar-to-hydrogen conversion. New materials and designs are making these processes more cost-effective and scalable [68].
   - Integration with Other Renewables: Combining solar-hydrogen plants with wind and other renewable sources can provide a more stable and reliable energy supply [69].
2. Economic Potential
   - Cost Reduction: As technology improves and scales up, the cost of producing green hydrogen is expected to decrease significantly. This will make it more competitive with traditional fossil fuels [70].
   - Job Creation: The development of solar-hydrogen infrastructure can create numerous jobs in manufacturing, installation, and maintenance [70].
3. Environmental Impact
   - Reduction in Greenhouse Gases: Solar-hydrogen plants produce hydrogen without emitting greenhouse gases, helping to combat climate change [71].
   - Sustainable Energy Storage: Hydrogen can be stored and used when solar energy is not available, providing a sustainable solution for energy storage.
4. Policy and Investment
   - Government Support: Many governments are implementing policies and providing funding to support the development of hydrogen technologies. For example, the European Union and Japan have strategic plans to integrate hydrogen into their energy systems [71].
   - Private Sector Investment: Increasing interest from the private sector is driving innovation and commercialization of solar-hydrogen technologies.
5. Global Adoption
   - International Collaboration: Countries are collaborating on research and development to accelerate the adoption of hydrogen technologies. This includes sharing best practices and technological innovations.
   - Market Expansion: The global market for green hydrogen is expanding, with significant growth expected in regions like Europe, Asia, and North America.

The future of solar-hydrogen plants looks bright, with ongoing advancements and increasing support from both the public and private sectors. These developments are paving the way for a cleaner, more sustainable energy future.

5. Experimental part and results

Also investigated were films of amorphous and nanocrystalline silicon-carbon alloy (a-nc-Si1-xCx:H (x = 0 ÷ 1)), doped with phosphorus (PH3) and boron (B2H6), obtained on various substrates of quartz, glass and silicon with a coating of Fe, Al, Pd, Ni, Ti, Ag.

Since Al and Ag have small diffusion barriers and poor surface wetting with single-wall carbon nanotubes (SWCNTs), they tend to aggregate and form large clusters. On the other hand, the binding energy between Fe and (SWCNTs) is high, but due to the high corrosion energy and poor wetting, Fe can form isolated clusters. Note that SWCNTs are obtained using a gas mixture of CH_4 and Ar. A jet of RF micro plasma is generated at atmospheric pressure using a single-tube electrode and directed onto a Fe-film-coated k-Si substrate.

By changing the synthesis parameters in a wide range (inner diameter of the electrode nozzle, methane flow rate and substrate temperature), carbon microstructures such as diamond particles, carbon nanowires, carbon nanotubes and cone-shaped Si microparticles were obtained.

The influence of growth conditions, methane flow rate and substrate type on the distribution of structures and properties of double-stage carbon nanotubes (DSCN) was also studied. At a flow rate of 600 cm^3/min, DSCN with predominantly semiconductor properties are obtained. At a higher flow rate (700 cm^3/min), a mixture of single-wall and double-wall nanotubes is formed, most of which are semiconductor. At lower rates (300 ÷ 500 cm^3/min), metallic multi-wall carbon nanotubes (MWCNTs) predominate. The length of the obtained nanotubes is 1 ÷ 4 µm [72].

It has been found that in films obtained from a gas mixture of $SiH_4+H_2+PH_3$ and $SiH_4+H_2+B_2H_6$ on a quartz or silicon substrate, with an increase in the concentration of PH_3, the average grain size (d) and the proportion of crystalline grains in volume (V_c) decrease. When doped with boron, with an increase in the concentration of B_2H_6, the value of d does not change, and V_c decreases [59].

In nanocrystalline SiC films with a thickness of 0.5 ÷ 1 µm, obtained in 80% H_2 +20% Ar plasma on a quartz substrate, with an increase in the substrate temperature from 200 to 600 °C, an increase in the density of SiC nanocrystals was observed, the average size of which was ~12 ÷ 24 nm [72]. The obtained results were also confirmed by the IR absorption spectrum method. Based on these results, it can be stated that monohydride Si–H and dehydride Si–H_2, in a complex, behave as a spatial barrier in the volume of films and change the growth of nanocrystals (Fig. 2) [72–75].

To analyze the pattern obtained on the Debyegram, we will use the Bragg-Wulf representation. To obtain a reflection of a certain order from some series of planes, the crystal must be oriented in such a way that these planes form an angle θ with the incident beam, satisfying the equation:

$$2d \sin \theta = n\lambda \tag{1}$$

Knowing the angle of incidence of the beam and the wavelength from equation (1), we can determine the diameter of the nanocrystals. Using formula (1) for each line, we can determine the ratio of the complex distance between the reflecting series of grids to the order of reflection:

$$\frac{d}{n} = \frac{\lambda}{2 \sin \theta} \tag{2}$$

The value $\frac{d}{n}$ for all lines is the final result obtained directly from the diagram.

Amorphous three-component alloys a-Si1-xCx:H were obtained from gas mixtures of SiH_4, CH_3, H_2. Hydrogen was added in the following ratios:

$$\frac{\left[\frac{PH_2}{SiH_4} + CH_4\right]}{H_2} = \frac{1}{20} \text{ for n} - \text{type films,}$$

$$\frac{\left[\frac{B_2H_6}{SiH_4} + CH_4\right]}{H_2} = \frac{1}{10} \quad \frac{\left[\frac{B_2H_6}{SiH_4} + CH_4\right]}{H_2} = \frac{1}{10} \text{ for p} - \text{type films.}$$

The films a-Si1-xCx:H and nc- Si1-xCx:H are obtained by deposition of

the gas mixture $[SiH_{4(1-x)}+CH_4]_x$. It is assumed that in the films, the relative content of carbon and silicon should correspond to the proportion: $\frac{(1-x)}{x}$. The alloyed layer was prepared as follows: $\frac{B_2H_6}{SiH_4+CH_4} = 0,$ 01 % and $\frac{PH_2}{SiH_4+CH_4} = 0,05 \%$, when x = 0 ÷ 1. Note that the obtained films also differ in morphology and structure.

An X-ray structural analysis of the obtained films was carried out, and an IR absorption spectrum was recorded on an IKS-29 spectrometer. Using the analysis of the half-width of the X-ray lines (the diffraction peak of reflection from the planes <111>, <220> and <311>), the average crystallite size (δ) was calculated, which for films with an area of 95 nm^2 and doped with phosphorus (at a high-frequency discharge power of $W_{rf} = 250$ W and a substrate temperature of $T_a = 600$ °C), was 12 nm.

The distances of X-rays from the planes <111> of crystalline silicon, the angular positions of the peaks 2θ, their height I_r and half-width Δ(2θ) for doped and undoped films differ (Fig. 5).

The figure shows the dependences of I_r, and Δ(2θ) for the maxima of X-ray reflection from the <220> planes of undoped nc–Si$_{1-x}$C$_x$:H films. With an increase in the annealing temperature in the range of 300–500 °C, the value of I_r increases monotonically, while the half-width Δ(2θ), which determines the size of nanocrystals, remains constant up to the annealing temperature $T_a = 500$ °C.This means that with an increase in the annealing temperature in the specified range, the number of nanocrystallites in the film increases, and their average size remains constant [74].

With further increase in the annealing temperature from T > 500 °C, the I_r rate increases sharply, and Δ(2θ) decreases at the same time, which indicates an increase in the size of nanocrystallites in the film. The results obtained for nc-Si$_{1-x}$C$_x$:H films from which hydrogen is completely removed, in this temperature range, were also verified by the method of IR absorption spectra. After heat treatment at 700 °C, with an increase in temperature, hydrogen effusion occurs, its concentration in the film decreases (Fig. 4, b).

However, in the case of a higher flow rate, about 700 cm^3/min, with an increase in the concentration of long-lived radicals, the mobility of ad atoms on the film surface increases, and the content of dihydrides (SiH$_2$) and hydrogen in it decreases, compared with films obtained at the same temperature in a high-frequency system. A decrease in the content of dihydrides, as shown in Ref. [76], leads to a decrease in the heterogeneity of the film microstructure, the number of centers without radiative recombination, and the density of localized states in the mobility gap. In the case of reactive magnetron sputtering, the minimum content of dihydrides is 20% relative to monohydrides (γ = SiH$_2$/SiH = 0,2) [76].

At different discharge densities, the relative carbon content in the films is greater than the relative carbon content in the gas mixture. This means that the reactive content of CH$_4$, compared to SiH$_4$, proceeds more effectively. However, with an increase in the power of high-frequency discharges, these values are equalized. The concentration of carbon and hydrogen in a-Si$_{1-x}$C$_x$:H films depends on the deposition conditions even in the case of unchanged content in the initial gas mixture of SiH$_4$, CH$_4$, H$_2$.

The obtained results show that in freshly deposited undoped films the nanocrystalline phase in the amorphous network is 70% of the total film volume. For phosphorus (PH$_3$) doped nc-Si$_{1-x}$C$_x$:H, films the total volume of crystallites in the film is 50%, while when doped with boron it is 30%. Similar results are also observed for the <220> and <311> planes of the silicon crystal lattice.

Fig. 6 shows the change in the deposition rate depending on the hydrogen pressure. As can be seen from the figure, the dependence takes a zero value at 5•10^{-4} Torr and as the gas pressure increases, the deposition rate increases. The deposition rate of 0.5 Å/s at a pressure of about 10^{-3} Torr was comparable to the data of the high-frequency deposition method.

Fig. 7 shows the dependence of the RF discharge power in high-pressure areas. Gas penetration also varied widely in high-pressure
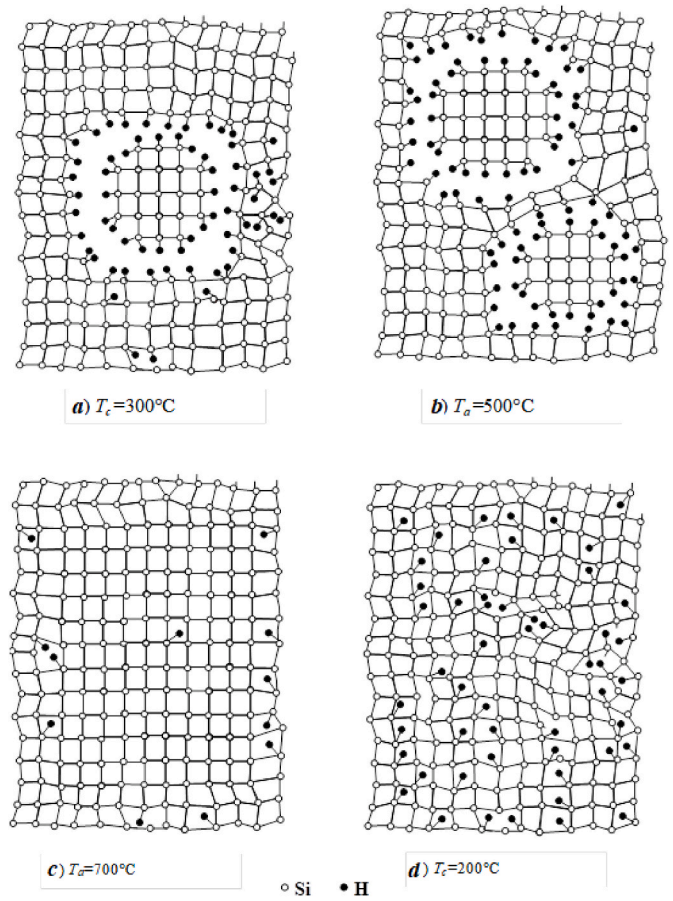
Fig. 4. (a, b, c, d). Schematic models for the structure of a-Si:nc-Si films.
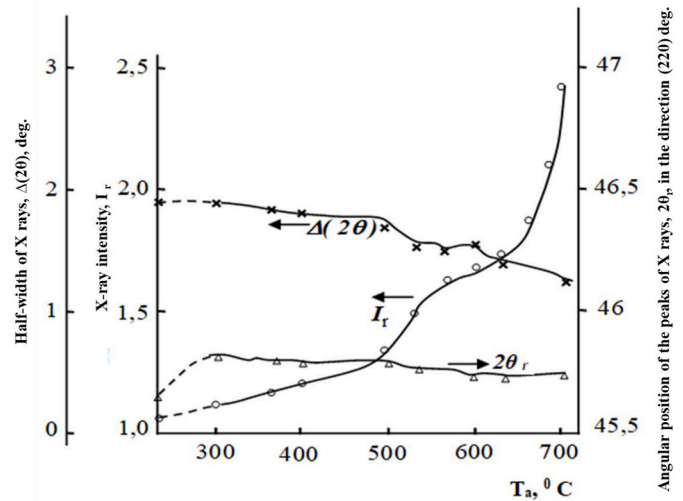
Fig. 5. Dependence of the I_r, $2\theta_r$ and Δ(2θ) values for the X-ray diffraction maximum along the (100) direction in undoped a-Si:H films on the annealing temperature T_a.

areas, since the initial gas pressure was constant (5•10^{-4} Torr). The gas pressure is regulated by a valve. With an increase in the RF discharge power, the gas pressure decreases and becomes constant in the range of 100–250 W. This phenomenon is not observed in an argon gas discharge and repeats the result of dissolution and reaction of the gas mixture due to the high-frequency discharge.
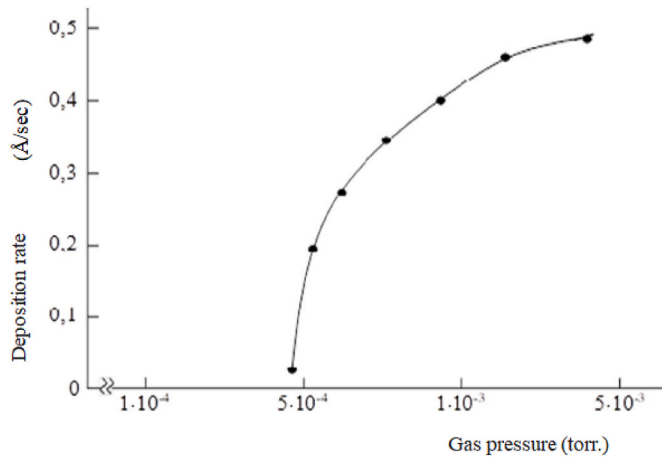
Fig. 6. Dependence of the deposition rate on the gas pressure when obtaining *a*-Si:H by magnetron sputtering.
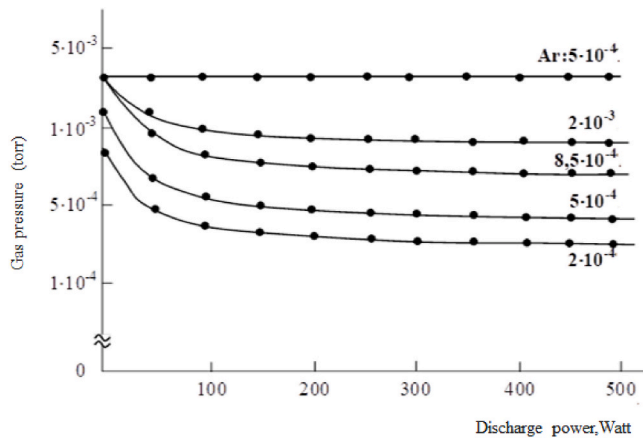
Fig. 7. The relationship between the discharge power and the gas pressure when producing *a*-Si:H films by magnetron sputtering.

Fig. 8 shows the relationship between the RF discharge power and the deposition rate. When the RF power is below 100 W, the deposition rate increases and gas penetration does not depend on the RF power. If the RF power is above 100 W, the deposition rate increases, but at high values, gas penetration increases sharply. This means that part of the gas is activated at high RF power values, and only the activated part reacts.
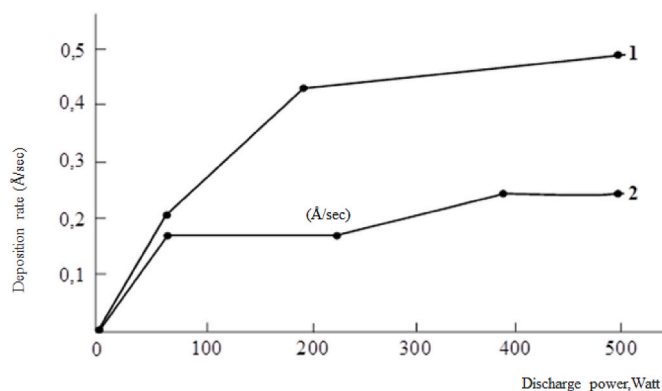
Fig. 8. Dependence between the deposition rate and the dicharging power when producing *a*-Si:H films by magnetron sputtering. Curves: 1 – films deposited at a vacuum of $5 \bullet 10^{-3}$ Torr, $2 - 5 \bullet 10^{-4}$ Torr. Substrate temperature $T = 300°C$

As a result of the work carried out, it can be concluded that deposition is controlled by the RF power at constant temperatures and a constant cathode potential.

Fig. 9 shows the temperature dependence of the activation energy of electrical conductivity (ΔE) for *a*-Si$_{1-x}$C$_x$:H. films. From these data it follows that in films obtained in a high-frequency discharge, the activation energy is greater than in the case of a low-frequency discharge [73]. In the first case, the dependence of the activation energy on the width of the forbidden band (E_a from $E_{g\ opt}$) is approximated by the equation:

$$E_a = 0.5\ E_{g\ opt}.$$

As can be seen from the data presented, the temperature range of electrical conductivity is not of a hopping nature, but of an activation nature. In this case, the concentration of paramagnetic centers has a low value and, depending on the hydrogen pressure ($P_{H2} = 0 \div 4.0$ mTorr), varies within the range of $10^{18} \div 10^{16}$ cm^{-3} eV^{-1}. At sufficiently low temperatures ($T \leq 80$ K), one could expect a hopping conductivity mechanism, as is inherent in all amorphous materials, including *a*-Si$_{1-x}$C$_x$:H [73,80,82–84].

Fig. 10 shows the IR absorption spectra of amorphous *a*-Si$_{1-x}$C$_x$:H films produced by magnetron sputtering in an RF system. As can be seen, three main absorption regions are observed in the infrared region of the spectrum: a broad peak at 760 cm^{-1}, resembling a shoulder in shape; peaks at 1000 cm^{-1}, respectively, relate to the stretching vibrations of the Si–C and the rocking vibrations of the CH$_4$ group attached to the silicon atom and the stretching mode of the C–H bond in the region of 2800–3000 cm^{-1} [73,80].

Fig. 11 shows the IR absorption spectra of amorphous *a*-Si:H films obtained at hydrogen pressures of: $P_{H_2} = 0.6$ mTorr; 1.4 mTorr; 2.4 mTorr; 3.8 mTorr.

As can be seen from Fig. 8, the absorption band for SiH monohydride corresponds to 2000 cm^{-1}, and for SiH$_2$ dehydride, it corresponds to 2100 cm^{-1} and 875 cm^{-1} [77,78].

Fig. 12 shows the optical absorption edge (α) in phosphorus-doped *a*-Si$_{1-x}$C$_x$:H films (x = 0 ÷ 0.32). The optical absorption coefficient (α) for phosphorus-doped a-Si:H approaches 105 cm-1, and with an increase in carbon content (x = 0 ÷ 0.32) its value decreases to 6104 cm^{-1}.

In order to determine the width of the forbidden zone, the dependence $(\alpha h\nu)^{1/2}$ on the photon energy $h\nu$ was constructed. The optical absorption coefficient is expressed by the relation (3). It was found that in the interval x = 0 ÷ 0.32 the width of the forbidden zone corresponds to $E_0 = 1.75 \div 2.14$ eV, and below E_0 in all the studied samples the absorption changes exponentially with energy and is determined by
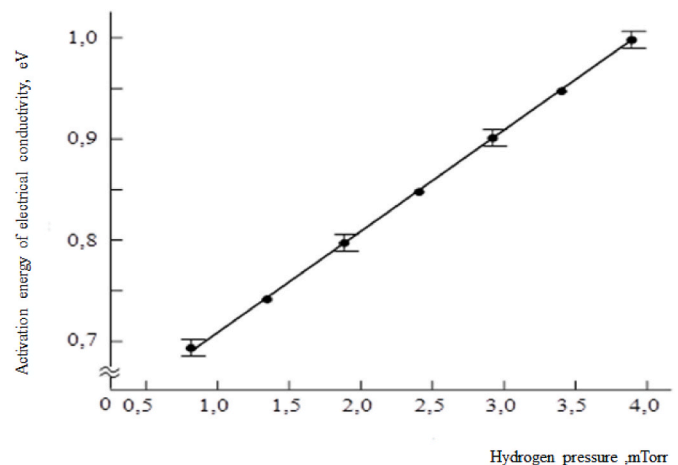
Fig. 9. Dependence between the activation energy of electrical conductivity and hydrogen pressure in the production of *a*-Si:H films by magnetron sputtering.
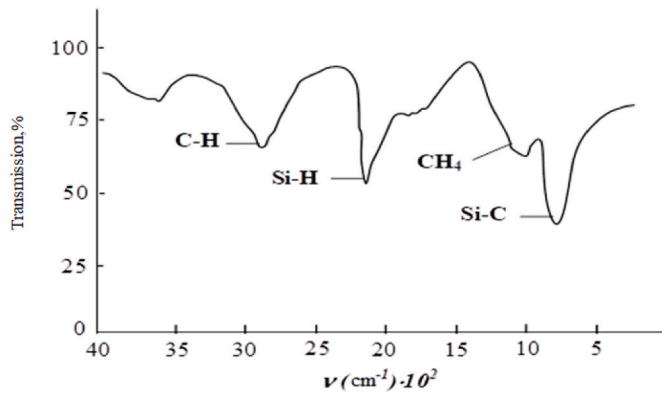
Fig. 10. IR absorption spectra for *a*-Si$_{1-x}$C$_x$:H ($x = 0,25$) films.
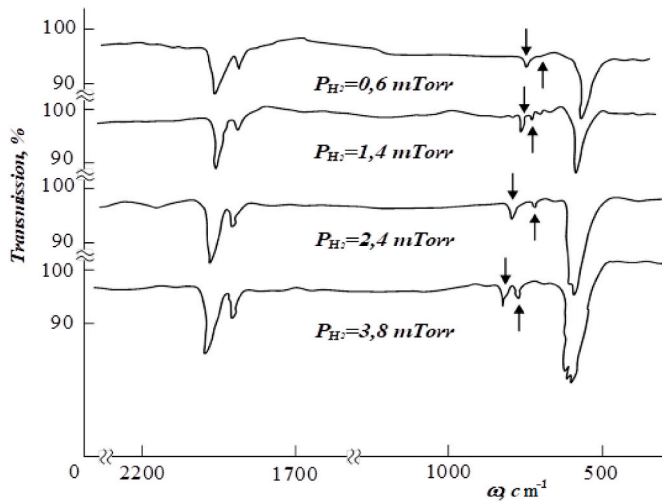
Fig. 11. IR absorption spectra of amorphous *a*-Si:H films obtained at hydrogen pressures of: P_{H_2} = 0.6 mTorr; 1.4 mTorr; 2.4 mTorr; 3.8 mTorr.
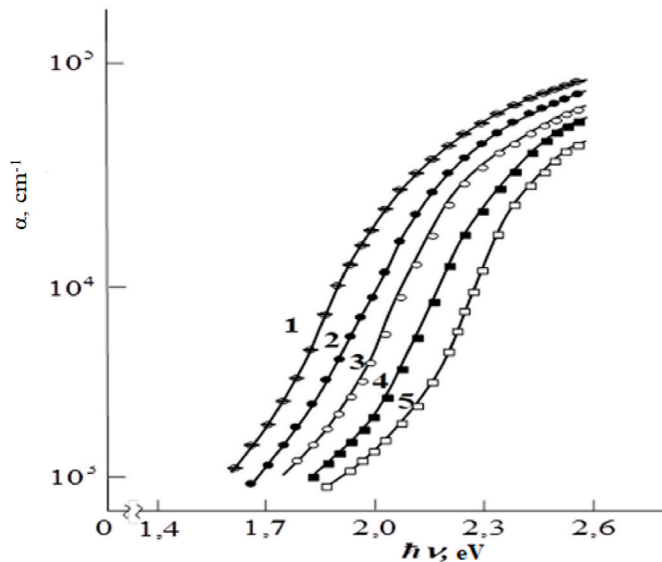
Fig. 12. Dependence of the optical absorption coefficient α on the photon energy *hν* for a-*a*-Si$_{1-x}$C$_x$:H ($x = 0 \div 1$) films doped with phosphorus.

formula (6). The Tauc model [78–81] is used to determine E$_0$.

$1 - x = 0$; $2 - x = 0,06$; $3 - x = 0,17$; $4 - x = 0,25$; $5 - x = 0,32$. The conditions of the modes are described in the text.

IR absorption spectra were calculated using the formula:

$$T = \frac{(1 - R_1)(1 - R_2)(1 - R_3)\exp(-\alpha d)}{(1 - R_2 R_3)\left\{1 - \left[R_1 R_2 + R_1 R_2(1 - R_2)^2\right]\right\}\exp(-2\alpha d)} \quad (3)$$

where R$_1$, R$_2$, R$_3$ are the reflection coefficients for air-film, film-substrate and substrate-air interactions, respectively. For strongly absorbing regions R$_1$=R$_2$=R$_3$=R, determined by the band gap width E$_0$.

The film thickness d with a known refractive index is determined under the conditions of interference phenomena. To avoid complex calculations and to avoid interference phenomena, silicon substrates are used. When using a silicon substrate, the absorption coefficient outside the fundamental absorption edge region is determined by the formula below [79,81]:

$$T = \frac{4T_0^2 e^{-\alpha d}}{(1 + T_0)^2 - (1 - T_0)^2 e^{-2\alpha d}}, \quad (4)$$

Here T is the film transmittance, and T$_0$is the silicon substrate transmittance, T = T$_0$ = 0.54; n$_{sub}$ = n$_{film}$ = 3.42, (α = 0).

Equation (4) is true with an error of ±10% at αd≥0.1. From equation (3), the reflection coefficients R1, R2, R3 are theoretically determined by the relationships for different types of substrate:

$$R_1 = |(n - 1)^2 + k_0^2| / |(n + 1)^2 + k_0^2|$$
$$R_2 = |(n - n_1)^2 + k_0^2| / |(n + n_1)^2 + k_0^2|, \quad (5)$$
$$R_3 = |(n_1 - 1)| / |(n_1 + 1)|^2$$

n and n$_1$ (=1.5) show the refractive indices of the film and substrate, respectively. Here $k_0^2 \ll (n - 1,5)^2$ (this relationship is valid for weakly absorbing regions of light).

In most amorphous materials, including *a*-Si:H films and its alloys at photon energies below E$_0$, in all the studied samples, absorption changes exponentially with energy and is described by the formula:

$$\alpha = \text{const}\exp[-\beta(E_1 - h\nu)], \quad (6)$$

where const = 4π/nc; n is the refractive index determined from the position of the interference peaks in the transmission and reflection spectra, c is the speed of light, E$_1$ is the energy of the order of E$_0$. β does not depend on the temperature near 300 K and is determined by the formula β ∼ 0.8/kT. The optical absorption coefficients α were determined by the following formulas from equation (3):

$$\alpha = \frac{1}{d}\ln\left[\frac{1}{2T}\left(\sqrt{(1 - R)^4 + 4R^2 T^2} + (1 - R)^2\right)\right], \quad (7)$$

$$P = \frac{(1 - R)^2}{T}; \quad \alpha = \frac{1}{d}\ln\frac{1}{2}\sqrt{(P^2 + 4R^2 + P)}. \quad (8)$$

It should be noted that expressions (8) are working formulas for determining the absorption coefficient of films on different substrates and at different wavelengths. When using a silicon substrate, the optical absorption coefficients are determined as follows:

$$e^{-\alpha d} = x; e^{-2\alpha d} = x^2,$$
$$T(1 + T_0)^2 - T(1 - T_0)^2 e^{-2\alpha d} - 4T_0^2 e^{-\alpha d},$$
$$T(1 - T_0)^2 x^2 + 4T_0^2 x - T(1 + T_0)^2 = 0,$$
$$e^{-\alpha d} = x = \frac{-2T_0^2 \pm \sqrt{4T_0^4 - T^2(1 - T_0^2)^2}}{T(1 - T_0)^2} - \alpha d = \ln x; \quad \alpha = -\frac{1}{d}\ln x. \quad (9)$$

6. Creation of solar cells

Amorphous films of *a*-Si:H and their alloys are often used for the production of electronic devices [59,61–63,71–74]. Such alloys are characterized by two phases: amorphous and nanocrystalline, the most interesting of which are the phases located at the boundary of crystallinity, which are considered the most stable for the creation of electronic devices.

A cascade element with a glass structure//ITO/p$^+$-*a*-SiC:H/i-*a*-Si:H/n$^+$-nk-Si:H/p$^+$-nk-Si:H/i-nk-Si:H/n$^+$-nk-Si:H/Ag/Al was obtained as follows: a layer of p-type *a*-SiC:H, which plays the role of a window, doped with boron [B$_2$H$_6$/(SiH$_4$+CH$_4$) = 0,1%] and 300 Å thick is deposited on a transparent conducting film of indium-tin oxides (ITO), pre-sputtered onto a glass substrate.

Then, an undoped *i*-layer of *a*-SiC:H with a thickness of d = 5000 Å was deposited, followed by the application of a layer of n-type nc-Si doped with phosphorus (PH$_3$/SiH$_4$ = 0.5%) with a thickness of 400 Å. In the same way, the subsequent layer of p$^+$-nk-Si:H, i-nk-Si:H, n$^+$-nk-Si:H was deposited by the above-mentioned method. The contact of Ag/Al alloys was applied last.

When using a too thin « window» (for radiation output), the open circuit voltage (V$_\infty$) increases, and when the «window» is too thick, the short-circuit current density (J$_{sc}$) increases. Therefore, an optimal thickness for the «window» is selected.

It is the largest V∞ and Jsc that are obtained with a «window » thickness of 300 Å. This, in turn, characterizes the efficiency of the elements. The optical absorption coefficient (α) for the *i*-layer in the visible region of the spectrum reaches 8 10^4 cm^{-1} and is described by the relationship:

$$\sqrt{\alpha h\nu} = B(h\nu - E_C), \tag{10}$$

where the coefficient B = 530 eV^{-1} cm^{-1} is determined by extrapolation of the linear dependence $\sqrt{\alpha h\nu}$ on the photon energy $h\nu$; E$_0$ = 1.85 eV is the width of the forbidden band.

To obtain the photovoltaic effect, the cells were illuminated by a light source with an intensity of ~100 mW/cm^2, in the wavelength range of 300–900 nm. An element with an area of 1.2 cm^2 had the following characteristics: V$_\infty$ = 0.882 V, J$_{sc}$ = 18.0 mA/cm^2, fill factor (ξ) = 0.709, efficiency (η) = 11.2% (Fig. 10, curve 2). The cells were illuminated with a photon flux of N = 10^{17}–18^{18} m^{-2} s^{-1} in the short-circuit mode. The carrier collection efficiency (CE) Y(λ) at different wavelengths was determined as the ratio of the number of incident photons to the number of free carriers collected by the external circuit [75,76].

$$Y(\lambda) = J_p(\lambda) /e N(\lambda) \tag{11}$$

where J$_p$(λ) is the photocurrent density, has a value of 10 mA/cm^2, N(λ) is the flux of incident photons, e is the charge of free carriers.

Highly efficient solar cells were obtained in a similar manner // ITO/p$^+$YH/i − a − Si : H/n$^+$ − nk − Si : H/p$^+$ − nk − Si : H/ i − nk − − Si : H/n$^+$ − nk − Si : H/Ag/Al. After film deposition, a transparent conductive film coating with 80% visible light transmittance was used as the front contact. A 300 Å thick layer of p$^+$ type SWCNTs doped with boron [B$_2$H$_6$/(SiH$_4$+CH$_4$) = 0,1 %] and acting as an optical window was deposited on a quartz plate.

Amorphous three-component alloys *a*-nk- Si$_{1-x}$C$_x$:H were obtained from gas mixtures of SiH$_4$, CH$_4$, H$_2$. Hydrogen was added in the following ratios: [B$_2$H$_6$/(SiH$_4$+CH$_4$)/H$_2$ = 1/10] for p-type SWCNT films. The composition of p-type films obtained by reactive magnetron sputtering deposition at a substrate temperature of 500^{0}C is characterized by an excess of carbon. Depending on the temperature, deposition rate and thickness of the resulting film, localized carbon can be either amorphous or crystalline. When studying the photovoltaic effect, an element with an area of 1.0 cm^2 had the following characteristics: V$_\infty$ = 0.98 V, J$_{sc}$ = 19.0 mA/cm^2, fill factor (ξ) = 0.8, efficiency (η) = 14.09%
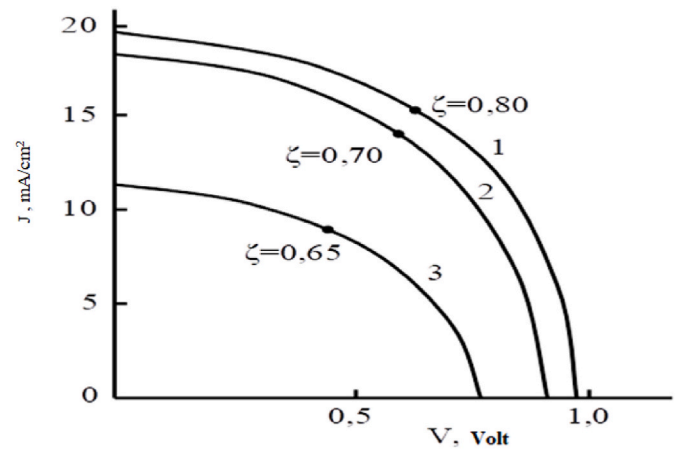
Fig. 13. Volt-ampere characteristics of solar cells: 1. cascade type UN/*a*-Si:H; 2. *a*-Si$_{1-x}$C$_x$:H/*a*-Si:H; 3. nc-*a*-Si:H.

(Fig. 13, curve 1).

Solar cells based on the Pt/*a*-Si:H Schottky barrier were also created. To improve the quality and reproducibility of the solar cell, a 300 Å thick n$^+$ layer of nanocrystalline Si was first deposited on the substrate. Then, a 5000 Å thick *i*-layer made of *a*-Si:H was deposited, and a 100 Å thick metal layer of Pt was deposited to obtain the barrier. Pd was used as the front contact, and a steel substrate was used for the back contact. Using the dependences of J$_{sc}$ on V$_\infty$ from the relation:

$$V_\infty = \frac{n'kT}{q}\ln\left(\frac{J_{sc}}{J_0} + 1\right) \tag{12}$$

the quality factor of the diode is determined as equal n' = 1, 58; 1, 9; 2, 2 for the Schottky barrier, the cascade solar cell UN/*a*-Si:H and *a*-SiC:H/*a*-Si:H, respectively.

The saturation current density of the diodes is determined by the formula:

$$J_0 = q\mu_C N_C E_C \exp\left(-\frac{\varphi_B}{kT}\right), \tag{13}$$

where $\mu_C = 20\ cM^2(V{\cdot}c)^{-1}$ is the electron mobility in the conduction band, $E_C = 10^4\ V/cm$, q is the electron charge [67,75,76]. The barrier height φ_B is determined using the expression [67,75,76]:

$$V_\infty = \frac{n'kT}{8}[\ln J_{sc} - \ln(q\mu_C N_C E_C)] + n'\varphi_B. \tag{14}$$

According to work [67], since $n' \approx 1\ \varphi_B = 1, 1$ eV.

From the capacitance-voltage characteristics [67,76], we find the value of the built-in potential $V_0 = 0, 42$ V and the space charge density $N \approx 3{\cdot}10^{15}$ cm^{-3}; then to determine the depletion layer, using the equation from Refs. [67,76] in the form:

$$W_e = \left(\frac{\xi}{2\pi q}\right)^{\frac{1}{2}}\left(\frac{V_0}{N}\right)^{\frac{1}{2}}, \tag{15}$$

we find that the width of the depleted layer is $W_e = 0, 35$ μm.

From curve 3 in Fig. 10, the value of the highest efficiency $\xi = 6, 05$ % and the best $J_{SC} = 12, 1$ mA/cm^2 was determined, at $V_\infty = 0, 77$ and $\zeta = 0, 65$.

Fig. 14 shows the dependence of the collection coefficient on the wavelength of light at a photon flux of ~10^{17}÷10^{18} m^{-2} s^{-1} in short-circuit mode. The efficiency of collecting charge carriers at different wavelengths was determined using equation (11).

To obtain cascaded *a*-Si:H/nc-Si:H solar cells, the study was conducted in a single chamber. To reduce contamination of the *i*- and p-layers of the cells, a 20-min pumping cycle is used before deposition. The
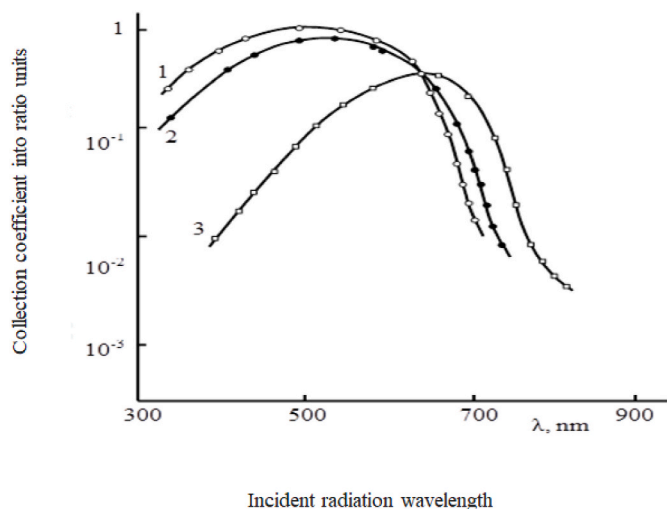
Fig. 14. Dependence of the collection coefficient on the wavelength of incident radiation: 1. cascade solar cell UN/a-Si:H; 2. cascade solar cell a-Si$_{1-x}$C$_x$:H/a-Si:H; 3. Schottky barrier solar cell.

i- and p-layers thoroughly isolate (in the form of B–P complexes) most of the P atoms on the chamber walls, which leads to high cell quality and minor degradation of performance. Unlike most manufacturing technologies, this method does not require cleaning the chamber after deposition of each p-layer.

7. Accumulation, storage, transportation of ENERGY at solar-hydrogen plants

Solar-hydrogen plants are an exciting area of renewable energy technology, combining solar power with hydrogen production, storage, and transportation (Fig. 15). Here's a brief overview of how these processes work:

Fig. 15. SOLAR-HYDROGEN ENERGY.(provided to the authors on 26.11.2024 for printing in IJHE from the archive of Fermaltech Montenegro Limited, made by A.L. Gusev using Designer. On the DALL E 3 platform.)

7.1. Accumulation

Solar energy is harnessed using photovoltaic (PV) panels or solar thermal systems. This energy is then used to power an electrolyzer, which splits water into hydrogen and oxygen through a process called electrolysis. The hydrogen produced can be stored for later use.

7.2. Storage

Hydrogen storage is a critical aspect of solar-hydrogen plants. There are several methods for storing hydrogen:

- Compressed Gas: Hydrogen gas is stored under high pressure in robust tanks.
- Liquid Hydrogen: Hydrogen is cooled to very low temperatures and stored as a liquid, which is more energy-dense but requires significant energy for cooling.
- Solid-State Storage: Advanced materials like metal hydrides, carbon-based materials, and metal-organic frameworks (MOFs) are used to store hydrogen in a solid form.

7.3. Transportation

Transporting hydrogen can be done in several ways:

- Pipelines: For large-scale distribution, hydrogen can be transported through pipelines, similar to natural gas.
- Tanker Trucks: Hydrogen can be transported in high-pressure tanks or as a liquid in cryogenic tanks.
- Hydrogen Carriers: Chemical compounds that can absorb and release hydrogen, making it easier to transport and store.

7.4. Integration with renewable energy

Integrating hydrogen production with solar and wind power can enhance the efficiency and reliability of renewable energy systems. For example, excess solar or wind energy can be used to produce hydrogen, which can then be stored and used to generate electricity during periods of low renewable energy production.

This combination of technologies not only provides a way to store and transport energy but also helps in reducing greenhouse gas emissions and promoting a sustainable energy future.

8. Safety issues of solar-hydrogen plants

Safety is a critical concern in the operation of solar-hydrogen plants due to the unique properties of hydrogen and the complexities of integrating solar energy systems. Here are some key safety issues:

1. Hydrogen Production
   - Electrolysis Risks: The process of electrolysis, which splits water into hydrogen and oxygen, involves high electrical currents and can pose risks of electric shock and arc flashes.
   - Gas Leaks: Hydrogen is highly flammable and can leak easily due to its small molecular size. Even small leaks can lead to significant hazards.
2. Hydrogen Storage
   - High Pressure: Storing hydrogen as a compressed gas requires high-pressure tanks, which can be prone to ruptures or leaks if not properly maintained.
   - Cryogenic Temperatures: Liquid hydrogen storage involves extremely low temperatures, which can cause materials to become brittle and increase the risk of leaks and explosions.
3. Hydrogen Transportation
   - Pipeline Integrity: Transporting hydrogen through pipelines requires materials that can withstand hydrogen embrittlement, a

process where hydrogen makes metals brittle and prone to cracking.

- Tanker Safety: Transporting hydrogen in tanker trucks involves risks of accidents and leaks, which can lead to fires or explosions.

4. General Safety Measures

- Fire and Explosion Risks: Hydrogen has a wide flammability range and low ignition energy, making it highly susceptible to fires and explosions.
- Safety Protocols: Implementing rigorous safety protocols, regular maintenance, and continuous monitoring are essential to mitigate these risks.

4. Regulatory Compliance

- Codes and Standards: Adhering to international codes and standards for hydrogen production, storage, and transportation is crucial for ensuring safety.

9. Production of new solar cells and their application in solar-hydrogen energy

The production of thin-layer silicon alloys and their application in solar-hydrogen energy is a rapidly advancing field. Here are some key points:

9.1. Production of thin-layer silicon alloys

1. Amorphous Silicon (a-Si) Thin Films: These are widely used in photovoltaic (PV) cells due to their low cost and ease of production. Amorphous silicon thin films are created using techniques like plasma-enhanced chemical vapor deposition (PECVD) and reactive magnetron sputtering.
2. Hydrogenated Amorphous Silicon (a-Si:H): This variant includes hydrogen to improve the material's electronic properties. It is commonly used in thin-film solar cells, which are part of the second generation of PV technology.
3. Nanocrystalline Silicon (nc-Si): This material combines the properties of crystalline and amorphous silicon, offering higher efficiency and stability. It is produced using similar deposition techniques but under different conditions to control the crystallinity.

9.2. Application in solar-hydrogen energy

1. Photovoltaic Cells: Thin-layer silicon alloys are used in PV cells to convert sunlight into electricity. These cells can be integrated with hydrogen production systems to create a sustainable energy cycle.
2. Hydrogen Production: The electricity generated by silicon-based PV cells can be used to electrolyze water, producing hydrogen. This hydrogen can then be stored and used in fuel cells to generate electricity when needed.
3. Hybrid Systems: Combining solar PV cells with hydrogen fuel cells creates a hybrid system that can provide continuous power. During sunny periods, the PV cells generate electricity directly, while excess energy is used to produce hydrogen. During cloudy periods or at night, the stored hydrogen is used to generate electricity.

These advancements in thin-layer silicon alloys and their integration into solar-hydrogen systems are crucial for developing sustainable and efficient energy solutions.

10. Conclusion

The results of this work show the prospects of obtaining films of amorphous and nanocrystalline silicon carbon deposited by the method of reactive magnetron sputtering. Experiments show that by changing the process parameters and conditions, amorphous films are deposited on various structural phases. It was also found that the process parameters (substrate temperature, film deposition rate, RF discharge power)

affect the physical properties of amorphous and nanocrystalline silicon carbon. The results of the studies carried out in this work show that a-Si$_{1-x}$C$_x$:H and nc-Si films are promising materials for creating cascade solar cells. And also the studied films are a promising material in micro and nano electronics.

Declaration of competing interest

There is no conflict of interest among the members of the authors' collective; the authors made an equal contribution to the work.

Acknowledgements

References

[1] Sacramento EM, Sales AD, Lima LC, Veziroglu TN. A solar-wind hydrogen energy system for the ceará state-Brazil. Alternat Energy Ecol (ISJAEE) 2019;7–9:32–42. https://doi.org/10.15518/isjaee.2019.07-09.032-042 (In Russ.).

[2] Sheffield JW. The extraordinary hydrogen romantic - the story of dr. T. Nejat Veziroglu Alternat Energy Ecol (ISJAEE) 2019;(4–6):12–3.

[3] Stolyarevsky AYa. System functions of hydrogen energy (preface to the paper by T. N. VEZIROGLU). Alternat Energy Ecol (ISJAEE) 2017;16–18:14–5. https://doi.org/10.15518/isjaee.2017.16-18.014-015 (In Russ.).

[4] Veziroglu TN, Sahin S. 21ST CENTURY'S energy: hydrogen energy system. Alternat Energy Ecol (ISJAEE) 2014;2:12–28 (In Russ.).

[5] Veziroğlu TN, Şahın S. 21st century's energy: hydrogen energy system. Alternat Energy Ecol (ISJAEE) 2019;4–6:14–27. https://doi.org/10.15518/isjaee.2019.04-06.014-027.

[6] Nowotny J, Veziroglu TN. Impact of hydrogen on the environment. Alternat Energy Ecol (ISJAEE) 2019;01–03:16–24. https://doi.org/10.15518/isjaee.2019.01-03.016-024.

[7] Almogren S, Veziroğlu TN. SOLAR-HYDROGEN energy system for Saudi Arabia. Alternat Energy Ecol (ISJAEE) 2018;7–9:30–42. https://doi.org/10.15518/isjaee.2018.07-09.030-042 (In Russ.).

[8] Gusev AL, Veziroglu TN. Twelve interviews with the legendary Patriarch of hydrogen energy prof. Dr. T.N. Veziroglu Main Concl Interview ? 1. Alternat Energy Ecol (ISJAEE) 2021;25–27:22–9. https://doi.org/10.15518/isjaee.2021.09.022-029 (In Russ.).

[9] Article E. Foreword of president, International Association for Hydrogen Energy T. Nejat Veziroglu Celebrating 14th Anniversary of International Scientific Journal for Alternative Energy and Ecology. Alternat Energy Ecol (ISJAEE) 2014;(14):12–3 (In Russ.).

[10] Gusev AL. In: GUSEV AL, editor. Foreword by the chief. Alternative Energy and Ecology (ISJAEE); 2021. https://doi.org/10.15518/isjaee.2021.04-06.012-020 (4-6):12-20. (Editorial, ISJAEE, #04-06, February, 2021) (In Russ.).

[11] Gusev AL. In: Gusev AL, editor. Foreword by the chief editor. Alternative Energy and Ecology (ISJAEE); 2021. https://doi.org/10.15518/isjaee.2021.09.014-021 (25-27):14-21. (Editorial, ISJAEE, #025-027, September, 2021) (In Russ.).

[12] Veziroğlu TN, Escher WJ. Solar energy utilization in advanced residential and commercial applications through hydrogen energy. Alternat Energy Ecol (ISJAEE) 2018;7–9:10–29. https://doi.org/10.15518/isjaee.2018.07-09.010-029 (In Russ.).

[13] Bockris JO, Veziroglu TN. Estimates of the price of hydrogen as a medium for wind and solar sources. Alternat Energy Ecol (ISJAEE) 2018;10–12:34–42. https://doi.org/10.15518/isjaee.2018.10-12.034-042 (In Russ.).

[14] Goltsov VA, Veziroglu TN. From hydrogen economy to hydrogen civilization. Alternat Energy Ecol (ISJAEE) 2017;22–24:25–32. https://doi.org/10.15518/isjaee.2017.22-24.025-032 (In Russ.).

[15] Goltsov VA, Veziroglu TN. A step on the road to hydrogen civilization. Alternat Energy Ecol (ISJAEE) 2017;22–24:33–9. https://doi.org/10.15518/isjaee.2017.22-24.033-039 (In Russ.).

[16] Ramenskiy AYu. FORTY-FIVE years of selfless service to the ideals of solar-hydrogen energy: the first president of the international association of hydrogen energy, professor T. nejat veziroglu IS 95 years old. Alternat Energy Ecol (ISJAEE) 2019;(01–03):12–4 (In Russ.).

[17] Sacramento EM, Sales AD, Lima LC, Veziroglu TN. A solar-wind hydrogen energy system for the ceará state-Brazil. Alternat Energy Ecol (ISJAEE) 2019;7–9:32–42. https://doi.org/10.15518/isjaee.2019.07-09.032-042 (In Russ.).

[18] Nowotny J, Bak T, Chu D, Fiechter S, Murch GE, Veziroglu TN. Sustainable practices: solar hydrogen fuel and education program on sustainable energy systems. Alternat Energy Ecol (ISJAEE) 2017;22–24:14–24. https://doi.org/10.15518/isjaee.2017.22-24.014-024 (In Russ.).

[19] Nowotny J, Hoshino T, Dodson J, Atanacio AJ, Ionescu M, Peterson V, Prince KE, Yamawak M, Bak T, Sigmund W, Veziroglu TN, Alim MA. Towards sustainable energy: generation of hydrogen fuel using nuclear energy. Alternat Energy Ecol (ISJAEE) 2017;22–24:63–82. https://doi.org/10.15518/isjaee.2017.22-24.063-082 (In Russ.).

[20] Contrerasa A, Possob F, Veziroglu TN. Modeling and simulation of the production of hydrogen using hydroelectricity in Venezuela. Alternat Energy Ecol (ISJAEE) 2018;22–24:88–95. https://doi.org/10.15518/isjaee.2018.22-24.088-095.

[21] Alexander L. Gusev, Aydin M. Gafarov, Panah H. Suleymanov, Ibrahim A. Habibov, Rauf Kh Malikov, Yashar H. Hasanov, A.I. Levina, Pavel Mikheev, Ruslan A. Ufa,.

[22] Some aspects of reliability prediction of chemical industry and hydrogen energy facilities (vessels, machinery and equipment) operated in emergency situations and extreme conditions. Int J Hydrogen Energy 2024;86:482–510. https://doi.org/10.1016/j.ijhydene.2024.07.462. ISSN 0360-3199, https://www.sciencedirect.com/science/article/pii/S0360319924032002.

[23] Gusev AL, Jabbarov TG, Mamedov ShG, Malikov Rauf, Hajibalaev NM, Abdullaeva SD, Abbasov NM. Production of hydrogen and carbon in the petrochemical industry by cracking of hydrocarbons in the process of heat utilization in steel production. Int J Hydrogen Energy 2023;48(40):14954–63. https://doi.org/10.1016/j.ijhydene.2022.12.341. ISSN 0360-3199, https://www.sciencedirect.com/science/article/pii/S0360319922062280.

[24] Gusev AL. Thermodynamic peculiarities of low-temperature regeneration of cryosorption devices in heat-insulation cavities of hydrogenous cryogenic tanks. Int J Hydrogen Energy 2001;26(8):863–71. https://doi.org/10.1016/S0360-3199(01)00024-6. ISSN 0360-3199, https://www.sciencedirect.com/science/article/pii/S0360319901000246.

[25] Ufa RA, Malkova YY, Gusev AL, Ruban NY, Vasilev AS. Algorithm for optimal pairing of res and hydrogen energy storage systems. Int J Hydrogen Energy 2021;46(68):33659–69. https://doi.org/10.1016/j.ijhydene.2021.07.094. ISSN 0360-3199, https://www.sciencedirect.com/science/article/pii/S0360319921027567.

[26] Zhiznin SZ, Shvets NN, Timokhov VM, Gusev AL. Economics of hydrogen energy of green transition in the world and Russia.Part I. Int J Hydrogen Energy 2023;48(57):21544–67. https://doi.org/10.1016/j.ijhydene.2023.03.069. ISSN 0360-3199, https://www.sciencedirect.com/science/article/pii/S0360319923010832.

[27] https://en.wikipedia.org/wiki/William_Grylls_Adamshttps://truesouthsolar.net/history-of-photovoltaic-energy/.

[28] https://en.wikipedia.org/wiki/Charles_Frittshttps://www.solarfeeds.com/mag/fritts-legacy-unveiling-the-first-solar-cell/.

[29] https://www.nobelprize.org/prizes/physics/1921/summary/https://www.nobelprize.org/prizes/physics/1921/einstein-facts/.

[30] https://www.nobelprize.org/prizes/physics/1921/einstein/facts/https://www.edn.com/einstein-wins-1921-nobel-prize-in-physics-november-9-1922/.

[31] https://www.nobelprize.org/prizes/physics/1921/einstein/facts/https://www.edn.com/einstein-wins-1921-nobel-prize-in-physics-november-9-1922/.

[32] https://ethw.org/Milestones:First_Practical_Photovoltaic_Solar_Cellhttps://www.science.org.au/curious/technology-future/solar-pv.

[33] https://ethw.org/Milestones:First_Practical_Photovoltaic_Solar_Cellhttps://www.science.org.au/curious/technology-future/solar-pv.

[34] https://en.wikipedia.org/wiki/Turhan_Nejat_Veziro%C4%9Fluhttps://www.life.illinois.edu/govindjee/Electronic%20Publications/2016/T_Nejat_Veziro_lu%20%282016%29.pdf.

[35] https://en.wikipedia.org/wiki/Turhan_Nejat_Veziro%C4%9Flu.

[36] https://en.wikipedia.org/wiki/Turhan_Nejat_Veziro%C4%9Flu.

[37] https://www.life.illinois.edu/govindjee/Electronic%20Publications/2016/T_Nejat_Veziro_lu%20%282016%29.pdf.

[38] https://www.cambridge.org/core/journals/environmental-conservation/article/abs/solarhydrogen-energy-system-the-choice-of-the-future/D0A17DDE86F0AB3085C1EC3333985535.

[39] https://en.wikipedia.org/wiki/Turhan_Nejat_Veziro%C4%9Flu.

[40] https://www.life.illinois.edu/govindjee/Electronic%20Publications/2016/T_Nejat_Veziro_lu%20%282016%29.pdf.

[41] https://www.cambridge.org/core/journals/environmental-conservation/article/abs/solarhydrogen-energy-system-the-choice-of-the-future/D0A17DDE86F0AB3085C1EC3333985535.

[42] https://www.researchgate.net/profile/Martin-Green-7.

[43] https://www.unsw.edu.au/newsroom/news/2021/01/australian-father-of-photovoltaics-awarded-prestigious-2021-japa.

[44] https://pubs.aip.org/aip/apl/article/55/13/1363/55817/22-8-efficient-silicon-solar-cell.

[45] https://www.mdpi.com/2071-1050/13/22/12508.

[46] https://scholar.google.com/citations?user=hDS2pfEAAAAJ.

[47] https://www.researchgate.net/profile/Alexander-Gusev-5.

[48] https://www.calameo.com/books/00685263119b65dba802d.

[49] https://wiki.naturalphilosophy.org/index.php?title=John_M_Bockris.

[50] Bockris JOM, Veziroglu TN, Smith D. Solar hydrogen energy: the power to save the earth. Optima-book; 1991. https://books.google.me/books?id=zwwKAQAMAAJ. Optima.

[51] https://www.mdpi.com/2411-9660/7/4/97.

[52] https://www.researchgate.net/publication/372868967_The_Status_of_On-Board_Hydrogen_Storage_in_Fuel_Cell_Electric_Vehicles/fulltext/64cbc769d394182ab3a

[53] 11a88/The-Status-of-On-Board-Hydrogen-Storage-in-Fuel-Cell-Electric-Vehicles.pdf.

[53] https://www.wasserstoffrat.de/en/national-hydrogen-council/members/schaefer.

[54] Afanasyev VP, Gudovskikh AS, Nevedomskii VN, et al. Effect of heat treatment on the structure and properties of a-Si:H films obtained by cyclic deposition. FTP 2002;36:238–43.

[55] Golikova OA, Kazanin MM, Kudoyarova VKh. Staebler-Wronski effect depending on the position of the Fermi level and doped amorphous hydrogenated silicon. FTP 1998;32:484–9.

[56] Mezdragina MM, Abramov AV, Mosina GM, et al. Effect of annealing in an atomic hydrogen atmosphere on the properties of amorphous hydrogenated silicon films and the parameters of p-i-n structures based on them. FTP 1998;32(5):620–37.

[57] Golikova OA, Babakhodzhaev US. Crystallization of amorphous hydrogenated silicon films deposited under different conditions. FTP 2002;36:1259–62.

[58] Bonifoulen A, Edely M, Kassiba A. Structure and optical characteristics of nanocrystalline silicon carbide. Physics B 2011;406(3):4500–4.

[59] Najafov BA, Figarov VR. Hydrogen content evaluation in hydrogenated nano crystalline silicon and its amorphous with germanium and carbon. Int J Hydrogen Energy 2010;35:4361–7.

[60] Sinelnikov BM, Tarala VA, Mitchenko IS. Study of the influence of synthesis temperature on the microstructure of thin films of silicon carbide synthesized from trimethyl chlorosilane vapors.//Perspective of the material, Special issue. New Mater Technol 2007;2:547–50.

[61] Kimura F, Asaka K, Nakahara H, Kakai F, Saito YJ. Transmission electron microscopy study of mass transport and electricity in a carbon nanotube containing a Cu nanorod. Nanosci Nanotechnol 2010;(6):3907–9.

[62] Zhihus H, Xianba Z, Hogwei D, Cai Y, Shibin C, et al. Hydrogenated p-type nanocrystalline silicon in amorphous silicon solar cells. J Non-Cryst Solids 2006;9–20(352):1900–3.

[63] Tune DD, Flavel BS, Krupke R, Shopter JG. Solar cells based on carbon nanotubes (CN) with Si.//Carbon nanotube – silicon solar cells. Adv Energy Mater 2012;(9):1043–55.

[64] Buzanovsky VA. Review. Gas sensors based on carbon nanotubes, vol. 2. Engineer's Handbook; 2012. p. 2–30.

[65] https://www.dissercat.com/content/vliyanie-uslovii-osazhdeniya-v-protsesse-magnetronnogo-raspyleniya-na-strukturu-i-svoistva.

[66] Najafov BA. Production of various types of nanotubes (OUN, DUN, MUN) and the effect of substrate temperatures of nanocrystalline silicon-carbon deposited by reactive magnetron sputtering. "Actual Problems of Physics" Vl Republican Conference. Opto, nanoelectronics, condensed matter and high energy physics. Baku: BSU; 2012. December 14-15.

[67] https://applied-research.ru/ru/article/view?id=9956.

[68] https://pubs.acs.org/doi/pdf/10.1021/acsenergylett.1c02591.

[69] https://academic.oup.com/ce/article/8/2/1/7617398.

[70] https://academic.oup.com/ce/article/8/2/1/7617398.

[71] https://pubs.acs.org/doi/pdf/10.1021/acsenergylett.1c02591.

[72] Najafov BA, Isakov GI. Optical and electrical properties of amorphous a-Si1-xCx:H. Inorg Mater 2010;46(6):624–30.

[73] Nadzhafov BA, Dadashova VV. Optoelectronic properties of thin films of hydrogenated amorphous silicon-carbon and nanocrystalline silicon. Ukr Phys J 2013;58(10):369–974.

[74] Peng Yingcai, Jiang Zirang, Wang Fend, Ma Lei, Lai Jianzhang. Study and prospects of nanostructured solar cells. Mikronano-Electr Tecnal 2011;48(8):481–8.

[75] Mezdragina MM, Golikova OA, Kazanin MM, Kudoyarova VKh. Inorg Mater 1991;27(4):816–9.

[76] Nadzhafov BA. Production of amorphous hydrogenated silicon carbide a-Si1-xCx:H (x=0÷1) for photovoltaic converters. ISAEE 2007;11(33):177–9.

[77] Nadzhafov BA. Photosensitive effects in amorphous films a-Si0.80Ge0.20:Hx. ISAEE Solar Energy 2005;3(33):59–63.

[78] Najafov BA, Isakov GI. Properties of amorphous a-Si1-xGex:H (x=0÷1) films. Inorg Mater 2009;45(7):713–8.

[79] Dutta R, Banerjee PK. Optical and electrical properties of hydrogenated amorphous silicon carbide. Phys Status Solidi 1982;113:277–84.

[80] Najafov BA, Isakov GI. Optical properties of amorphous films of a-Si1-xGex:H solid solution with different hydrogen concentrations. ZhPS 2005;72(3):371–6.

[81] Meden A, Sho M. Physics of application of amorphous semiconductors. Moscow: Mir; 1991.

[82] Najafov BA, Fiqarov VR. Int J Sustain, Energy 2007;26(4):7.

[83] Najafov BA, Nasirov ShN, Neimetov SR. General characteristics of amorphous silicon alloys. Hydrogenation, crystallization and polymerization. Alternat Energy Ecol (ISJAEE) 2024;7:21–40.

[84] Nadzhafov BA, Nasirov ShN, Nasirov ShN. Optical properties of thin films a-Si1-xGex:H (x = 0 ÷ 1) for electronic devices. Alternat Energy Ecol (ISJAEE) 2024;(8):18–29.